Title
Longitudinal instability of slurry pipeline flow

Authors
Samson, René
Biello, Joseph Anthony

Publication Date
2017-04-01

Peer reviewed

International Journal of Multiphase Flow 90 (2017) 57–63

Contents lists available at ScienceDirect

International Journal of Multiphase Flow

journal homepage: www.elsevier.com/locate/ijmulflow

Longitudinal instability of slurry pipeline flow

René Samson[a,*], Joseph A. Biello[b]

[a] Retired scientist
[b] Department of Mathematics, University of California, Davis, CA 95616, USA

ARTICLE INFO

Article history:
Received 23 October 2016
Revised 19 December 2016
Accepted 19 December 2016
Available online 23 December 2016

Keywords:
Slurry transport
Hydrodynamic instability
Hindered settling
Pipeline plugging

ABSTRACT

This paper deals with the flow of solid/liquid mixtures through long-distance pipelines. Such flows can be destabilized by the formation of local plugs which may impede or even block the flow. Plugs may develop at the interface between regions of different mean concentration. The driving force for the development of such plugs is the existence of local gradients of the axial flux of solids.

A mathematical model is developed which describes this mode of plug formation in slurry pipelines. Several assumptions and approximations enable us to reduce the 3D continuity equation of the solid particles to an effective 1D-equation that contains a concentration-dependent flux function. The latter equation is solved numerically.

Illustrative calculations lead to the conclusion that the accumulation of material in a plug does not continue without limit but instead levels off at values that are pumpable under most practical conditions, provided that a certain margin of overdesign is in place.

1. Introduction

Pipelines transporting a mixture of finely ground solids and liquid ("slurry") are used in the mining industry to move minerals such as coal and metal ores from remote mining locations to installations (power plants, refining plants) where they are first separated from the carrier fluid and then further processed. In operational practice these slurry pipelines occasionally suffer from plug formation. Such events are often ascribed to bad design or maloperation. However, plugging incidents have occasionally been reported when none of the latter causal factors play a role.

In the nineteen-fifties, Wasp and Cook (1960) analysed a number of plugging incidents relating to a 108-miles long pipeline transporting coal slurry from mines in southern Ohio to Lake Erie in Northern Ohio. A condition for smooth transport is that the flow velocity in the pipeline exceeds a critical value, so that the flow turbulence is sufficient to keep even the coarsest particles in suspension. Wasp and Cook's analysis revealed that even when this condition was satisfied there were occurrences of plugging. The phenomenon described by Wasp and Cook can be explained as follows. Consider a slurry pipeline; assume that along its central axis there is an abrupt decrease of the solids concentration in the direction of the flow (see Fig. 1). Envisage a cylindrical volume element along a short length of the pipe axis that covers the entire pipe cross-section and that straddles the zone of the concentration jump. As will be demonstrated later, the flux of solids into the volume element at the upflow face might exceed the outflow from the opposite end. Assume now that the volume element moves with the average velocity of the flow. Given enough time, the accumulation of solid material inside the volume element could in principle proceed to the point where the plug becomes unpumpable.

By which mechanism could such an initial concentration drop along the pipe axis come about? Although the spontaneous creation of concentration gradients (during steady operation) as a result of random fluctuations can never be ruled out completely, there are far more probable causal mechanisms relating to operational factors. For example: if the pipeline is laid out in hilly terrain with substantial elevation differences, accidental or intentional shutdowns or slowdowns could lead to massive demixing of the solid particles and the carrier liquid, with heavier material accumulating in the valleys and lighter zones at the higher elevations. Restarting such a pipeline implies operation in a mode where substantial concentration differences might exist along the pipe axis.

In the next section, a mathematical model is formulated that describes the dynamics at the interface between a dilute and a dense zone, as shown in Fig. 1. The starting point for this development is the 3D continuity equation for the solid particles in the flowing solids/fluid mixture. Several assumptions and approximations enable us to reduce the 3D continuity equation of the solid

* Corresponding author.
E-mail addresses: rsamsonjvlk@gmail.com (R. Samson), biello@math.ucdavis.edu (J.A. Biello).

http://dx.doi.org/10.1016/j.ijmultiphaseflow.2016.12.005
0301-9322/

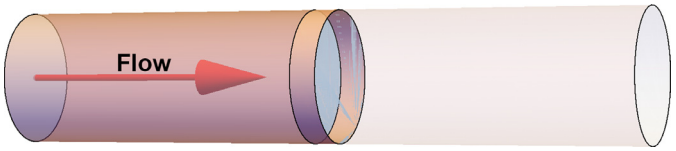

Fig. 1. Sketch of a slurry pipeline with a longitudinal concentration gradient.

particles to an effective 1D-equation. In Section 3, the solution of this equation is reviewed. In Section 4, the results and the most important practical consequences of the model are summarized. A somewhat similar 1D equation was derived by van Rhee and Talmon in the context of dredging applications (see van Rhee and Talmon (2010)).

2. Mathematical model

Our starting point is the equation of conservation of mass of the solid particles in the fluid. Assume that the solid particles are subdivided into a discrete number of size classes. Each size class i ($i = 1, 2, \ldots, n$), obeys a mass conservation law of the form

$$\frac{\partial C_i}{\partial t} + \vec{\nabla} \cdot (\vec{u}\, C_i - \nu\, \vec{\nabla} C_i) = 0. \tag{1}$$

Here, C_i is the fractional concentration of solids of size class i (C_i will be expressed in terms of concentration *by volume* rather than by weight), $\vec{u}$ is the flow velocity vector, ν is a diffusivity parameter and t is time. The coordinate system is so chosen that the pipe axis is along the x-axis and the vertical direction is along the z-axis. The axial component of the velocity vector, u_x, is assumed to be a given function of the radial pipe coordinate (orthogonal to the pipe axis), to be specified later on (see Eq. 12). The radial and azimuthal components of the velocity field will be shown to be inconsequential in the present model (see Appendix A). The diffusivity parameter ν is assumed to be dictated by the turbulence of the flow and it is also assumed to be a given constant (see Appendix B).

Eq. 1 is now integrated over the pipe cross-section. A cross-sectionally averaged concentration c_i is defined which only depends on x and t:

$$c_i(x,t) = \frac{1}{A}\int C_i(\vec{r},t)\; dA \equiv \frac{1}{\pi R^2}\int_0^R r dr \int_0^{2\pi} d\theta \quad C_i(x,r,\theta,t). \tag{2}$$

Here, r and θ are radial and azimuthal pipe coordinates and R is the pipe radius.

Without further simplifications, the cross-sectional averaging would turn the 3D-PDE Eq. 1 into a complicated 3D-integro-differential equation which would hardly be of any practical use. By the introduction of a number of physically plausible assumptions however, Eq. 1 can be turned into a much simpler 1D-PDE depending only on x and t. The first and most crucial simplification is the following one:

$$\int u_x C_i\; dA \approx \int u_x \gamma_i\; dA, \tag{3}$$

where γ_i is the solution of an ordinary DE

$$w_i \Omega_i(c)\gamma_i + \nu \frac{\partial \gamma_i}{\partial z} = 0, \tag{4}$$

$c = \sum_{i=1}^n c_i$, w_i is the single-particle settling velocity and $\Omega_i(c)$ is a function (to be specified later; see Eq. 27) that describes the influence that particles have on each other's settling velocity through steric hindrance. Eq. 4 is supplemented by the auxiliary condition that

$$(1/A)\int \gamma_i\; dA = c_i. \tag{5}$$

The physical meaning of this approximation is as follows. In Eq. 3, we effectively replace C_i (a function of x, r, θ, t) in the integral kernel by γ_i (a function of z alone). The concentration function γ_i is determined by the condition that there is no net transport of material in the vertical direction (Eq. 4). Downward convective fluxes (settling) and upward diffusive fluxes (turbulent mixing) are assumed to be balanced everywhere in the pipe and at all times. This implies that if a concentration gradient is transported along the pipe axis, then at each point x along the axis, *instantaneously* a situation of *local equilibrium in the z-direction* is established such that Eq. 4 holds true. The condition Eq. 5 ensures that at each point x and at each time t, the average values of γ_i and of C_i are equal.

If the z-dependence of Ω_i is ignored, then Eq. 4 can be easily solved:

$$\gamma_i/c_i = a_i \exp[-k_i z/R], \tag{6}$$

where

$$k_i = k_i(c) = R w_i \Omega_i(c)/\nu \tag{7}$$

and a_i is determined by Eq. 5:

$$1/a_i = (1/A)\int \exp[-k_i z/R]\; dA. \tag{8}$$

As will be shown later (see Appendix B), in many cases of practical interest the following inequality holds:

$$k_i \ll 1. \tag{9}$$

This can be used to expand a_i and γ_i in powers of k_i:

$$a_i = 1 - k_i^2/8 + \mathcal{O}(k_i^4) \tag{10}$$

and

$$\gamma_i/c_i = 1 - k_i z/R + k_i^2\; [\; (1/2)(z/R)^2 - (1/8)\;] + \mathcal{O}(k_i^3). \tag{11}$$

In reality, the vertical distribution of solid material is more complicated than suggested by Eqs. 6 and 11 (for more details on this point, see e.g. Barnard and Binnie (1963), Karabelas (1977), Kaushal and Tomita (2002) and Kaushal and Tomita (2013)).

A further approximation is the assumption that the axial velocity $u_x(r)$ obeys a "similarity-law"-type dependence on the radial pipe coordinate:

$$u_x(r) = \bar{u} + u^* F(r/R), \tag{12}$$

where

$$\bar{u} = (1/A)\int u_x(r)\; dA, \tag{13}$$

and u^* is a suitably chosen root-mean-square velocity fluctuation parameter. This law is generally accepted for single-phase turbulent pipe flow (see Tennekes and Lumley (1972)), but it is not quite right for slurries, where gravitational settling breaks the axial symmetry of the flow. For very dense slurries however, the degree of vertical inhomogeneity of the solids is relatively minor and therefore the deviations from axial symmetry in the velocity profile may be ignored.

From Eqs. 11 through 13 we obtain

$$(1/A)\int u_x \gamma_i\; dA = \bar{u} c_i - \epsilon k_i^2 u^* c_i, \tag{14}$$

where

$$\epsilon = (-1/2)\int_0^1 x^3 F(x)\; dx. \tag{15}$$

The dimensionless number ϵ is shown to be positive in Appendix B.

We now return to the cross-sectional integration of Eq. 1. It can be shown that the only term of the $\vec{\nabla} \cdot (\ldots)$-term in Eq. 1 that survives the cross-sectional integration is the axial term; i.e. the radial

and the azimuthal terms are eliminated by the integration. The vanishing of the latter terms is a consequence of the divergence theorem, the continuity of the flux-function in the angular direction and the no-flux boundary condition through the pipe surface. Mathematical details are given in Appendix A.

The resulting equation is

$$\frac{\partial c_i}{\partial t} + \frac{\partial}{\partial x}\left[\bar{u}c_i - \epsilon k_i^2 u^* c_i - \nu \frac{\partial c_i}{\partial x}\right] = 0. \tag{16}$$

It is convenient to apply one further coordinate transformation:

$$x^* = (B/\nu)\ (x - \bar{u}t) \quad \text{and} \quad t^* = (B^2/\nu)\ t\ , \tag{17}$$

where

$$B = \epsilon u^* (R w_1/\nu)^2. \tag{18}$$

This allows us to rewrite Eq. 16 as follows:

$$\frac{\partial c_i}{\partial t^*} + \frac{\partial f_i}{\partial x^*} = \frac{\partial^2 c_i}{\partial x^{*2}}, \tag{19}$$

where

$$f_i = -\ \beta_i\ \Omega_i^2(c)\ c_i\ , \tag{20}$$

and

$$\beta_i = (w_i/w_1)^2. \tag{21}$$

With this coordinate transformation, the origin of the x^*-coordinate moves along the pipe axis with the average velocity of the flow. Moreover, the diffusivity parameter ν has dropped out of the equation as an explicit parameter; instead, it appears as a scaling parameter in the definition of the new coordinates x^* and t^*, rendering them dimensionless.

If the particle size classes are chosen in order of *decreasing* size, it follows that the β's are in order of diminishing magnitude and are all ≤ 1.

Eq. 19 still needs initial and boundary conditions. In the calculations in the next sections, the following auxiliary conditions are used

$$c_i(x^*, t^* = 0) = c_i^0(x^*) = \begin{bmatrix} c_{iL} & \text{if} \quad x < 0 \\ c_{iR} & \text{if} \quad x > 0 \end{bmatrix} \tag{22}$$

and

$$\lim_{x^* \to -\infty} c_i(x^*, t^*) = c_{iL}, \tag{23}$$

$$\lim_{x^* \to +\infty} c_i(x^*, t^*) = c_{iR}, \tag{24}$$

$$c_{iL/R} = \chi_i\ c_{L/R} \quad \text{for all size classes } i, \tag{25}$$

$$\sum_{i=1}^{n} \chi_i = 1, \tag{26}$$

where the χ_i's are mass fractions of solids of size class i.

Eq. 19 is the central result of this paper. It is a 1D approximation of the 3D continuity equation. It is a very well known equation in many branches of science, in particular in compressible gas dynamics and in chromatography, see Courant and Friedrichs (1948) and Aris and Amundson (1973). Notable features of Eq. 19 are:

- It is a *system* of equations where the coupling between the members $i = 1, 2, \ldots, n$ is effected by the settling function $\Omega_i(c)$ with $c = \sum_{i=1}^{n} c_i$.
- It is a *non-linear* system, where the non-linearity arises from the settling function $\Omega_i(c)$.

The special features of this system, to be discussed below, are absent when there is only one single size class or when $\Omega_i(c)$ is simply a constant. The function $\Omega_i(c)$ is assumed to be a monotonically decreasing function of c:

$$\Omega_i(c) = (1 - c)^{\alpha_i}, \tag{27}$$

implying that the settling rate of the solid particles decreases as the concentration increases; for further details, see Section 3.2.

The central claim of this paper, namely: that plugs could develop at the interface between two zones of different density, provided that $c_L > c_R$ can now be clarified by rewriting Eq. 19 in an approximate form (where we temporarily ignore diffusive contributions):

$$\frac{\partial c_i}{\partial t^*} \approx -\frac{\partial f_i}{\partial x^*} \approx -\frac{f_i(x_2^*) - f_i(x_1^*)}{x_2^* - x_1^*} \tag{28}$$

Assume that $x_2^* > x_1^*$ and that x_2^* is located in a dilute zone and x_1^* in a dense zone. In the dilute zone, the *absolute value* of the flux $|f_i|$ will be larger than in the dense zone, on account of Eq. 27 (the magnitude of f_i is dominated by Ω_i rather than by c_i). Since both f's are negative, it follows that $\partial c_i/\partial t^* > 0$, i.e. species i accumulates in the region between x_1^* and x_2^*. (The minus sign in Eq. 20 implies that all the fluxes are *negative* in the (x^*, t^*)-coordinate system).

3. Numerical solution

3.1. Numerical method

A solution code for Eq. 19 was implemented in Wolfram Mathematica. No specific solution method (with respect to e.g. explicit or implicit difference schemes) was dictated; it was left up to the Mathematica solver code to select the most efficient scheme.

The only numerical parameter that sometimes needed some "tweaking" was the Maximum Step Size (MSS). For long integration times, sometimes numerical instabilities would occur that would have to be resolved by reducing the MSS. Obviously, this would lead to longer run times.

Other than this, there were no special difficulties in obtaining converged solutions.

3.2. Estimation of parameters

The theory presented above contains a number of parameters that have to be fixed. Parameters that are related to the size distribution of the solids particles and their terminal fall velocities in the fluid are listed in Table 1. The selected size distribution designated as 1A is a reasonable (discretized) approximation to particle size distributions that are commonly used in coal slurry pipelines (see e.g. the particle size-distribution data given in Wasp and Cook (1960). The data marked 1B and 1C correspond to - respectively - a coarser and a finer particle size distribution than the one given in 1A.

In the calculation of the settling velocities it was assumed that the solid particles have a density of 1400 kg/m^3 and that the carrier fluid is water. The correlation for the terminal fall velocity of solid spherical particles cited in Clift, Grace and Weber (1978) was used.

For the powers α_i in the hindered settling function Ω_i (see Eq. 27), the data in Richardson and Zaki (1954) were used. Richardson and Zaki (1954) made a thorough study of the sedimentation of approx 100 μm sized solid particles in fluids of various densities and viscosities at various volume fractions of the solid material. They correlated the measured sedimentation velocities in the form of the earlier quoted hindered settling function,

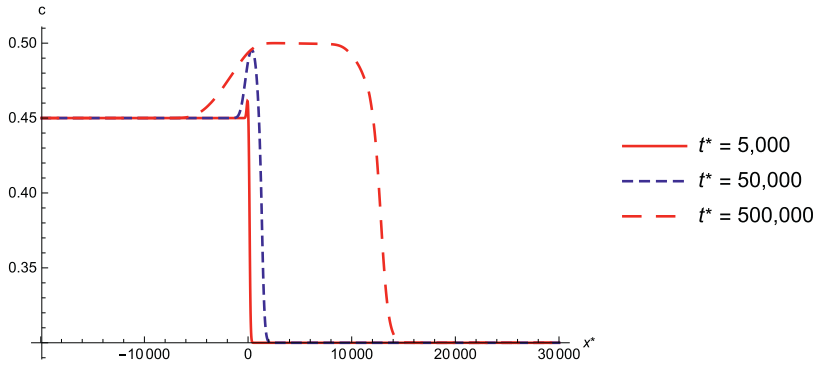

Fig. 2. Total solids concentration ($c = \sum_{i=1}^{n} c_i$) as a function of the space-like variable x^*; time t^* as parameter.

Table 1
Input parameters for the reported model calculations. The index i denotes the size class of the solid particles. The model includes three size classes. χ_i denotes the mass fraction of solids of size class i. d_i is the diameter of particles of class i. w_i is the (single-particle) terminal sedimentation velocity of particles of class i in the fluid. Re_i is the single-particle sedimentation Reynold's number $d_i w_i/\eta$, where η is the kinematic viscosity of the carrier fluid. α_i is the Richardson–Zaki parameter related to the hindered settling function Ω_i (see Eqs. 27 and 29) and $\beta_i = (w_i/w_1)^2$. Three cases are tabulated, corresponding to three different particle size distributions. Table 1A is the base case; Table 1B is a size distribution with larger particles; Table 1 C is a size distribution with smaller particles.

i	χ_i	d_i (μ m)	w_i (mm/s)	Re_i	α_i	β_i
1A						
1	0.2	600	34.8	20.9	3.284	1
2	0.5	300	14.0	4.20	3.855	0.162
3	0.3	75	1.21	0.091	4.650	0.00122
1B						
1	0.2	1200	76.2	91.5	2.833	1
2	0.5	600	34.8	20.9	3.284	0.208
3	0.3	150	4.56	0.685	4.400	0.00358
1C						
1	0.2	300	14.0	4.20	3.855	1
2	0.5	150	4.56	0.685	4.400	0.106
3	0.3	45	0.440	0.0198	4.650	0.000988

Eq. 27, the coefficient α_i being dependent on the Reynolds number based on the settling velocity of the particle:

$$\alpha_i = \begin{cases} 4.35\ Re_i^{-0.03} & \text{if} \quad 0.2 < Re_i < 1 \\ 4.45\ Re_i^{-0.1} & \text{if} \quad 1 < Re_i < 500 \end{cases} \tag{29}$$

with $Re_i = d_i w_i/\eta$, where d_i is the diameter of particles of class i, w_i is the (single-particle) terminal sedimentation velocity of particles of class i and η is the kinematic viscosity of the carrier fluid. Based on an extrapolation of the Richardson–Zaki data, $\alpha \to 4.65$ as $Re \to 0$.

3.3. Results and discussion

The initial axial concentration profile was assumed to be a sharp step change from $c_L = 0.45$ to $c_R = 0.30$. Using the parameters specified in Table 1A, the model was run. Results are shown in Figs. 2, 3 and 4. Fig. 2 clearly shows that an excess of mass accumulates at the interface and that this excess gradually increases with time. c_{max} (the maximum value of c over the plotted interval of x^*) is plotted against time in Fig. 3. The plot shows that the density of the plug approaches an asymptote. The maximum in the excess concentration is seen to be $c_{max}^{\infty} \approx 0.50$. Here, c_{max}^{∞} is the value of $c_{max}(t)$ as $t \to \infty$.

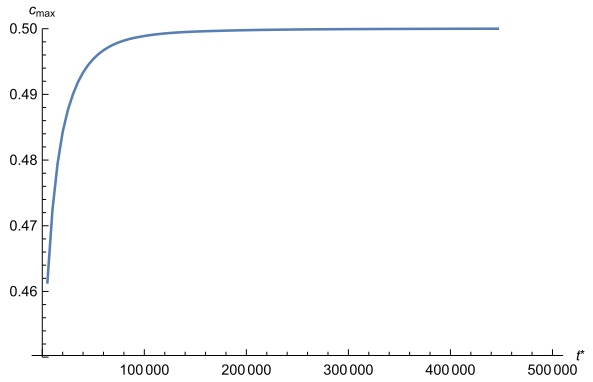

Fig. 3. The maximum concentration of c (c_{max}; maximum over x^*) as a function of time t^*.

The growth of the plug is rather slow. At $t^* = 5000$ (this corresponds to roughly 20 min of real time; see Appendix B.2), the blip at the interface is still hardly perceptible. It takes several hours for this growth to become substantial: only around $t^* = 10^5$ (corresponding to roughly 7 h) has the plug approached its asymptotic maximum value. At, say, 1.5 m/s average flow velocity and 7 h of flow, a distance along the pipe axis of about 35 km would have been covered.

The behaviour of the individual size fractions is shown in Fig. 4. It is seen that the main culprit for the mass accumulation is the heaviest size fraction. This stands to reason: *that* fraction is mainly responsible for the vertical inhomogeneity of the concentration distribution in the pipe cross-section. By contrast, the lightest fraction is very well-behaved (monotonic dependence of c_3 on x^*), while the middle fraction has a profile that is somewhat ambivalent.

A number of sensitivity tests were performed to establish how the results are affected by changes in the input parameters. Investigated were:

- the influence of the values of the left- and rightmost asymptotic concentrations c_L and c_R on c_{max}; refer to Table 2;
- the influence of the particle settling parameters on c_{max}; the size of the particles was varied as specified in Tables 1A, B and C.

Table 2 shows the results of the sensitivity study regarding the influence of c_L and c_R on c_{max}. From Fig. 3 it is clear that the calculations have to be extended to large values of t^* to get accurate data for c_{max}. In general, we aimed at a maximum value of t^* (t_f^*) equal to a few times 10^5. Up to values of t_f^* of about 10^4, we never encountered any numerical instabilities, however at values

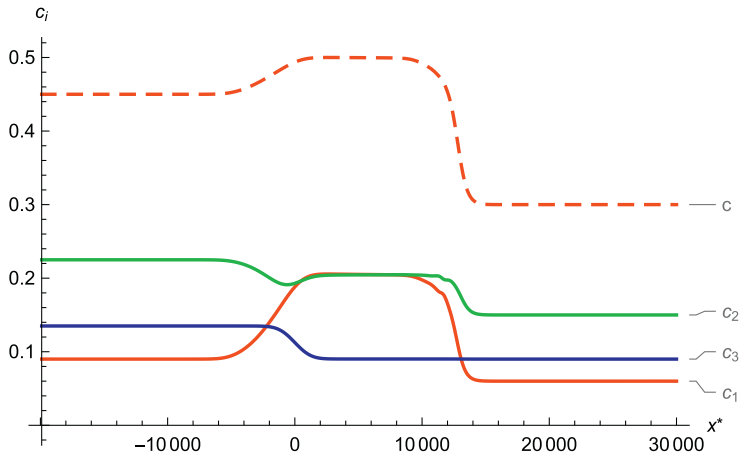

Fig. 4. The concentrations of the individual size classes c_i as a function of x^* at time $t^* = 500,000$.

Table 2
The influence of the values of the left- and rightmost asymptotic concentrations c_L and c_R on c^{∞}_{max}. $\Delta c^{\infty}_{max} = c^{\infty}_{max} - c_L$. Regarding the significance of the parameters t^*_f and MSS, see the body of the text for explanatory remarks.

c_L	c_R	$t^*_f * 10^{-5}$	MSS	c^{∞}_{max}	Δc^{∞}_{max}
0.45	0.40	3	50	0.471	0.021
0.45	0.30	5	50	0.500	0.050
0.45	0.15	2	5	0.523	0.073
0.45	0.05	2	5	0.528	0.078
0.30	0.20	4	25	0.341	0.041
0.30	0.05	2	5	0.346	0.046
0.55	0.40	6	50	0.588	0.038
0.55	0.25	3	25	0.607	0.057

of $t^*_f > 10^4$, sometimes instabilities would creep in, especially in cases where the difference between c_L and c_R was relatively large. In such cases we would be obliged to reduce the Maximum Step Size (MSS; see Table 2), obviously at the expense of longer run times. Ultimately, the choice of values to use for t^*_f and MSS is a compromise between accuracy and run time, but in all the reported data on c^{∞}_{max}, the error is *certainly* < 0.01 and *very probably* < 0.003.

The most prominent trend emerging from Table 2 is that the height of the hump Δc^{∞}_{max} correlates positively with the concentration gap $(c_L - c_R)$. This is not unreasonable: if $(c_L - c_R) \to 0$, the height of the hump should also $\to 0$, since in that case there is no driving force for the formation of the hump.

An additional test of the theory is a consideration of what happens when c_L is *smaller* (rather than larger) than c_R. Earlier, we argued from Eq. 28 that the condition $c_L > c_R$ implies that mass should accumulate at the interface. In the opposite case, if $c_L < c_R$, we must conclude that a mass *deficit* should then develop at the interface.

This claim is borne out by calculation: see Fig 5. Apart from a rather sharp, deep trough for x^* roughly between − 2000 and + 7,000, there is a second rather extended flat minimum in the plot for x^* roughly between − 24,000 and − 2,000. The reason for the existence of this secondary minimum is not clear.

Tables 1B and C show input data relating to larger, respectively smaller solid particles than the ones specified in Table 1A (the "base case"). Calculations were carried out regarding these two new particle size distributions with $c_L = 0.45$ and $c_R = 0.30$. Surprisingly, it was found that the c^{∞}_{max}-results for the three cases are in a remarkably narrow band width: $c^{\infty}_{max} = 0.498 \pm 0.003$.

It would be wrong, however, to conclude that the particle size distribution (PSD) is irrelevant. Even though the PSD does not affect the value of c^{∞}_{max}, it *does* have a huge effect on the time required to build a plug with this density. The dimensionless time $t^* = 10^5$ (approximately equal to the time needed to reach the asymptotic level) corresponds to respectively approximately 0.3 h (case 1B: coarse PSD), 7 h (case 1A: base case) and 250 h (case 1C: fine PSD) in the three PSD cases, as demonstrated in Appendix B.2; the three PSD-cases being described in Table 1.

In conclusion: although asymptotically the three cases are similar (as far as the height of the hump is concerned), the establishment of the asymptotic condition proceeds *much* faster when the slurry particles are larger. Hence, in industrial practice, the consequences of this type of plug formation may be more dramatic for coarse than for fine slurries.

4. Conclusions

Slurry pipelines with long-range longitudinal (along the axis) concentration gradients may exhibit surprising behaviour. In certain situations, these concentration gradients may give rise to local plugs, containing anomalously high solids densities. Rather than dissolving with time as a result of turbulent mixing, such plugs may self-amplify and may become denser in time.

A mathematical model was developed to describe this phenomenon. The model was tested under conditions that are typical for industrial coal slurry pipelines. It was found that the described type of plugs is relatively mild in character. By this, we mean the following two things. First: the maximal increase in slurry concentration inside the plug is usually only a few volume percents. The exact height of the plug $(\Delta c^{\infty}_{max})$ is mostly dictated by the initial concentration jump $(c_L - c_R)$ between the solids-rich and the solids-poor part of the concentration profile, as illustrated in Table 2. A typical maximal increase in solids concentration at the interface between the two parts of the profile is 5 vol %. Secondly: the temporal development of these plugs is generally not very fast. The rate of plug growth is mostly dictated by the size of the coarsest particles in the slurry. For a typical coal slurry, the time required to accumulate several (say, 5) volume % of solids concentration at the plugging interface would take several hours, corresponding to, say, 30–40 km of traversed pipe length. For slurries that are considerably coarser than an "average" coal slurry, the accumulation time could be considerably shorter (say, half an hour or even less than that, rather than several hours), corresponding to considerably shorter traversed pipe lengths. For coarse slurries, fully-developed plugs could be present very soon after restart of

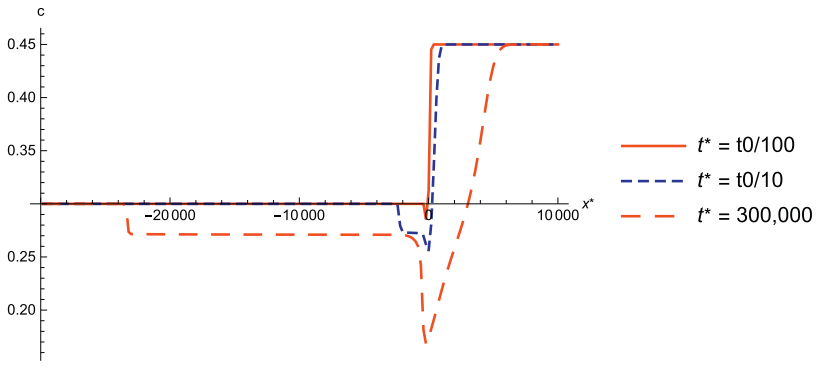

Fig. 5. Development of a mass *deficit* at the concentration interface for the case that $c_L < c_R$.

a dormant pipeline. An important learning point of the current model is that it points at the great importance of careful control of the top size of the solids particle size distribution.

Since most designers are inclined to incorporate a certain amount of "slack" in their designs so as to be able to handle minor increases of pressure drop in their pipelines, it is probable that they will naturally "design around" the plugging problem. In concrete terms this means that if the pipeline is intended to operate at a maximum solids concentration of, say, 45% by volume, the designer is well advised to base his design not on 45% but on, say 50% by volume, so as to be able to cope with potential short-lived plugs formed e.g. during pipe startup.

Acknowledgement

Part of this work was carried out while one of the authors (RS) was working at Shell Technology Center Amsterdam during the late nineteen-seventies.

Appendix A. Why do the radial and the azimuthal flux components drop out of Eq. 19?

Eq. 1contains a term of the form

$$\vec{\nabla}\cdot\vec{\Phi} \quad \text{where} \quad \vec{\Phi} = \vec{u}\,C_i - \nu\,\vec{\nabla}C_i. \tag{A.1}$$

In Eq. 19, only the axial flux term survives the cross-sectional averaging. What happened to the two other flux terms?

Denote cylindrical coordinates as $(x,\ r,\ \theta)$ where x is the axial coordinate, r the radial coordinate and θ the azimuthal (angular) coordinate. Averaging over the pipe's cross-section leads to the following integrals:

$$I_r = \int_0^{2\pi} d\theta \int_0^R dr\ \frac{\partial(r\Phi_r)}{\partial r} = \int_0^{2\pi} d\theta\ (r\Phi_r)|_{r=0}^{r=R}$$
$$= R\int_0^{2\pi} d\theta\ \Phi_r(R,\theta), \tag{A.2}$$

and

$$I_\theta = \int_0^R dr \int_0^{2\pi} d\theta\ \frac{\partial\Phi_\theta}{\partial\theta} = \int_0^R dr\,\Phi_\theta|_{\theta=0}^{\theta=2\pi}$$
$$= \int_0^R dr[\Phi_\theta(r,2\pi) - \Phi_\theta(r,0)]. \tag{A.3}$$

The vanishing of I_θ is easy to understand: if $\Phi_\theta(r,\ \theta)$ is a well-behaved (continuous) function, $\Phi_\theta(r,\ 2\pi)$ must obviously be equal to $\Phi_\theta(r,\ 0)$. The vanishing of I_r is a little bit trickier. Referring to A.1, the term u_rC_i must be zero at the pipe boundary $r = R$: there cannot be any flow perpendicular to the pipe wall. The same argument holds with respect to the $\vec{\nabla}C_i$-term: there cannot be any flow of (particle) mass out of the pipe wall, hence the radial component of $\vec{\nabla}C_i$ must vanish at $r = R$. Hence, I_r must vanish.

Appendix B. Estimation of some physical quantities occurring in the theory

In this appendix we present estimates of a number of quantities that are used in the model:

- the parameter ϵ (see Eq. 15);
- the diffusivity parameter ν, the parameter B (see Eq. 18) and the relation between dimensionless time t^* and physical time t (see Eq. 17);

and we provide evidence for:

- the claim made in Eq. 9 that $k_i \ll 1$.

B.1. The value of ϵ

In this Appendix, the parameter ϵ is calculated for a specific choice of the axial velocity profile, namely the so-called "1/7-profile" which is a good representation of (single-phase) turbulent pipe flow; see Bird, Stewart and Lightfoot (1960) :

$$u_x(y) = qu^*(1-y)^{1/7} \quad \text{where} \quad y = r/R. \tag{B.1}$$

Here, the constant q is related to the ratio $\bar{u}/u^*$:

$$\bar{u} = (1/A)\int u_x(r)\ dA = 2qu^*\int_0^1 y(1-y)^{1/7}dy$$
$$= 2qu^*B(2,8/7) = 2qu^*\frac{\Gamma(2)\Gamma(8/7)}{\Gamma(2+8/7)} = (98/120)qu^* \tag{B.2}$$

The beta function $B(a,\ b)$ and the gamma function $\Gamma(a)$ are as defined in Abramowitz and Stegun (1970). It follows that $q = (120/98)\cdot(\bar{u}/u^*)$. In Bird, Stewart and Lightfoot (1960), an approximate relation (the *logarithmic distribution*) is given, linking the ratio $\bar{u}/u^*$ to a turbulent Reynold's number based on u^*. From this relation, we estimate that at a distance of 0.25 m from the pipe wall, in a flow with an average velocity of 1.5 m/s, $\bar{u}/u^* \approx 30$, hence $q \approx 36.7$.

Now we tackle the calculation of ϵ:

$$\epsilon = (-1/2)\int_0^1 y^3F(y)\ dy = (-1/2)\int_0^1 y^3\frac{u_x(y)-\bar{u}}{u^*}\ dy$$
$$= (-1/2)\int_0^1 y^3\left[q(1-y)^{1/7} - \bar{u}/u^*\right]dy$$
$$= (-1/2)(\bar{u}/u^*)\left[(120/98)\int_0^1 y^3(1-y)^{1/7}dy - (1/4)\right]$$
$$= (-15)[(120/98)\cdot B(4,8/7) - (1/4)]$$
$$= (-15)[0.2304\ldots - 0.25] = +0.2939\ldots \tag{B.3}$$

B.2. The values of ν, B and t^*

An important parameter in the model is the turbulent diffusivity ν. It is commonly assumed in the theory of turbulence (see e.g. Tennekes and Lumley (1972)) that in turbulent pipe flow, ν can be approximately related to the pipe radius R and the turbulent rms velocity fluctuation u^* by $\nu = \zeta R u^*$. From the work reported in Barnard and Binnie (1963),Karabelas (1977), Kaushal and Tomita (2002) and Kaushal and Tomita (2013), it appears that the value $\zeta = 0.25$ is an adequate approximation. Assuming that $R =$ 0.25 m (i.e. for a pipeline with a diameter of 0.5 m) and u^* = 0.05 m s^{-1}, we get $\nu = 3.125 \times 10^{-3}\,m^2/s$. Using Eq. 18 and $w_1 = 0.0348\,m\,s^{-1}$ from Table 1A, we obtain $B = 0.114$ m s^{-1}. From Eq. 17, we then obtain that t(in seconds) $\approx 0.241\,t^*$. It follows that $t^* = 10^5$ corresponds to $t \approx$ 24,000 s, or $\approx$ 6.7 h.

Note that the ratio between t and t^* is sensitively dependent on the size of the particles; or - more precisely - on the free-settling velocity of the coarsest size fraction w_1 ($t/t^* \sim w_1^{-4}$). For the coarse particle size-distribution shown in Table 1B with $w_1 = 0.0762\,ms^{-1}$, we have t(in seconds) $\approx 0.01\,t^*$, or $t^* = 10^5$ corresponds to $t \approx$ 1050 s, or $\approx$ 0.3 h. Conversely, for the fine particle size-distribution shown in Table 1C with $w_1 = 0.0140\,ms^{-1}$, we have t(in seconds) $\approx 9.2\,t^*$, or $t^* = 10^5$ corresponds to $t \approx 9.2{*}10^5$ s, or $\approx$ 255 h.

A word of caution is in place regarding the reliability of the data discussed above. The conversion factor linking real time t(in seconds) and dimensionless time t^* is quite sensitively dependent on the value of ζ, namely: ($t/t^* \sim \zeta^5$). Consequently, relatively small variations in ζ can have a large impact on this conversion factor. From the existing papers on turbulent diffusivity of slurries in pipelines (see Barnard and Binnie (1963), Karabelas (1977), Kaushal and Tomita (2002) and Kaushal and Tomita (2013)), it is clear that the value of ζ used in the current study is by no means "cast in stone". This implies a certain degree of uncertainty in our statements regarding the time that is needed for plugs to develop to full maturity.

B.3. Proof that $k_i \ll 1$

In order to prove that $k_i \ll 1$, it suffices to show that this is true for $i = 1$ (the coarsest size fraction). Since the size fractions are in order of decreasing size, the inequality will certainly hold for the finer fractions if it is correct for $i = 1$. Using Eq. 27 for $c = 0.45$ and the power $\alpha_1 = 3.284$ (see Table 1), we calculate $\Omega_1 = 0.14$. It follows that $k_1 = 0.195$.

We conclude that for rather high concentrations ($c \approx 0.45$), the inequality holds true for all size fractions. For considerably smaller concentrations, the inequality would break down. However, in that case, the theory is not very relevant, as the system is then far removed from plugging.

References

Abramowitz, M., Stegun, I.A., 1970. Handbook of Mathematical Functions, 9th ed. Dover Publications.

Aris, R., Amundson, N.R., 1973. Mathematical methods in chemical engineering. First-Order Partial Differential Equations with Applications, Vol. 2. Prentice-Hall.

Barnard, B.J.S., Binnie, A.M., 1963. The vertical diffusivity and mean velocity of particles in a horizontal water pipe. J.Fluid Mech. 15, 35–48.

Bird, R.B., Stewart, W.E., Lightfoot, E.N., 1960. Transport Phenomena. John Wiley.

Clift, R., Grace, J.R., Weber, M.E., 1978. Bubbles, Drops, and Particles. Dover Publications.

Courant, R., Friedrichs, K.O., 1948. Supersonic Flow and Sound Waves. Interscience Publishers.

Karabelas, A.J., 1977. Vertical distribution of dilute suspensions in turbulent pipe flow. AIChE J. 23, 426–434.

Kaushal, D.R., Tomita, Y., 2002. Solids concentration profiles and pressure drop in pipeline flow of multisized particulate slurries. Int. J. Multiphase Flow 28, 1697–1717.

Kaushal, D.R., Tomita, Y., 2013. Prediction of concentration distribution in pipeline flow of highly concentrated slurries. Part. Sci. Technol. 31, 28–34.

Richardson, J.F., Zaki, W.N., 1954. Sedimentation and fluidisation: part I. Trans. Inst. Chem. Eng. 32, 35–53.

Tennekes, H., Lumley, J.L., 1972. A First Course in Turbulence. MIT Press.

van Rhee, C., Talmon, A.M., 2010. Sedimentation and erosion of sediment at high solids concentrations. In: Heywood, N. (Ed.), 18th International Conference on Hydrotransport, pp. 211–222.

Wasp, E. J., Cook, P. A. C., 1960. US Patent 2,920,923.